Exploring the gaits for debris removal and excavation with Klann-legged robots

S.Nandan, Email : Swastik Nandan <s.swastiknandan@gmail.com>

***Abstract*— Constant effort is being dedicated in building robots that can supplant laborious work performed by humans with automated mechanisms. In this regard a large number of researches have been dedicated to emulate gaits of legged animals. Debris removal and excavation are activities of human interest that can be achieved with gaits of animals. The Klann-mechanism based legged robots can act not only as robots that can access difficult terrains but also as robots that can remove debris and act for excavation purposes. In this work we have explored the various trajectories of the end-effector of the Klann mechanism that can be suitable for this purpose. The trajectory curve of the end-effector of Klann-mechanism has been generated by solving trigonometric equations that can produce a continuous curve as a function of the input angle φ. By varying the length of the links , perspicuity has been gained in achieving trajectory suitable for this purpose. Fruitful gaits pertaining to this purpose has been identified. With reconfigurable links, all these trajectories can be achieved by a single set of legs. The trend of the impact force with the angular velocity has also been identified. The study of the impact force for this purpose is crucial as it entails the removal of heavy and tough objects and the choice of materials for the links and end effector can accordingly be made. This study validates the possibility of achieving walking robots with reconfigurable links that can double-up as debris remover and excavator.**

I. Introduction

While legged robots have always been a choice for a variety of applications like accessing extreme and inaccessible terrains[1] , given their versatility in bio-mimicry , legged robots are also extremely capable of debris removal and excavation. For legged robots , various design approaches are there to generate gait patterns , which includes : biomimetic adaptations based on ground contact timing[2] , graph search approach[3] , mechanical energy constraints[4] ,zero moment point model [5] to name a few. Currently , extensive study is being carried out in generating gait by generating trajectory of the limbs of the robot. Reconfigurable foot traces using the Klann mechanism has already been explored with six distinct walking patterns identified [6] where in , the authors presents the Klann based reconfigurable design and implementation where a robot changes its structural morphology by changing its components and sub-assembly parameters to adapt to multi-terrain and multi-tasking by producing a wide set of novel gait patterns. An outline of the synchronization of the legs of a quadruped robots to maintain stability of the platform has also been provided [7]. In this work we have tried to revisit the previously identified trajectories and identified novel trajectories suitable for excavation purposes.

In previous studies , the trajectory of the end effector has been plotted by interpolation of polynomial equations. Our work is unique because we have defined the trajectory by solving trigonometric equations to plot the change is the position of end effector with change in the input angle. This approach eliminates the possibility of error in ascertaining values of co-efficient terms of polynomials during interpolation that occurs when sufficient data points are not available. This approach also provides valuable information regarding the choice of link lengths that will produce the desired trajectories.

The standard path of hydraulic excavators has been tracked in [8] which shows the cyclic nature of such curves. The 'return' region of the trajectory of the hydraulic excavator is essentially a vertical drop with increase in the acceleration along the y direction with descend. The previously identified trajectory for the digging gait [6] in Klann mechanism significantly resembles this curve.

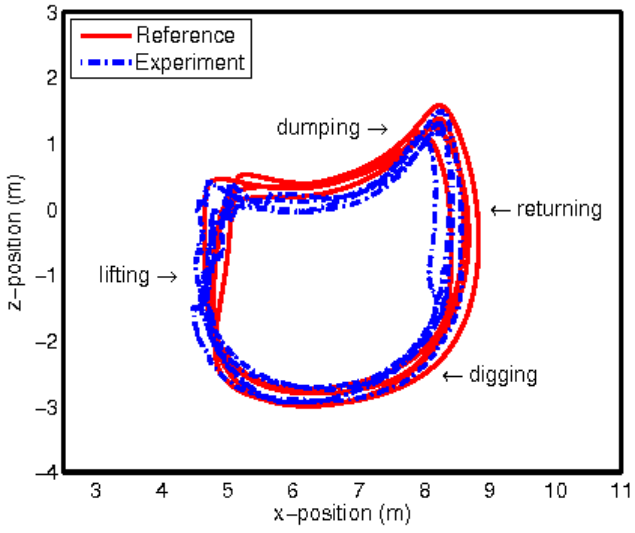

Figure 1 , ref [8] **Trejectory of a hydraulic excavator**

II. Problem Approach

In this study the position of the points O , G and D are fixed(figure 3). The input link is l_1, which undergoes complete rotation . It is the link adjacent to the fixed

link and it is the smallest link in the four bar linkage which include $l_1, l_3, l_2$and GO. GO is the fixed link. The link l_1 and the link l_2 acts as the crank and the rocker respectively. The lengths l_2, l_3, l_4, l_5, l_6 and l_7 can be varied using reconfigurable links to generate different gaits. In [9], reconfigurable leg hoppers has been identified as instruments for varying leg lengths in adaptive locomotion. The lengths l_1 along with the position of O , G and D are constants. The position of point O, G and D are invariable because they are points on the fixed link and the gap between these points cannot be varied in all practical purposes. In this approach the length of the input link has also been kept fixed for two reasons : l_1 needs to maintain the status of the smallest link in the l_1- l_3-l_2-GO four bar mechanism to ensure complete rotation , also l_1 is the smallest link and installation of reconfigurable link hoppers can be difficult at certain cases. The length of l_2 and l_3 can be varied as long as the Grashof's law is maintained. Link 3 and link 5 are stiff links hence angle α and β are constant for a specific model.

All the link lengths have been varied such that the end effector passes close to the ground level at least once in each cycle. The ground level has been ascertained in case I , which pertains to the default trajectory for walking. This ensures the stability of the platform of quadruped robots with proper synchronization , such that three legs of the robot are in touch with the ground while the other leg is up in the air [7].

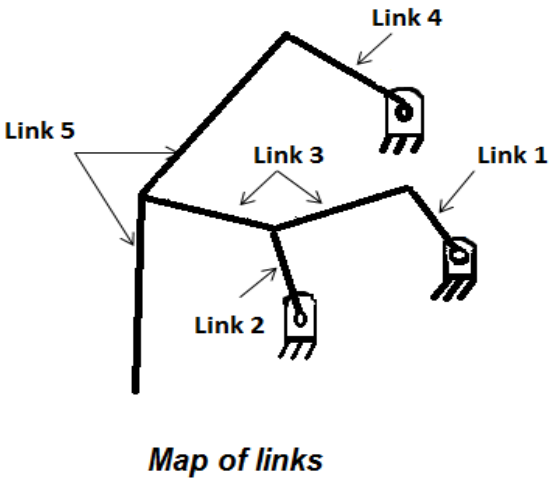

Figure 2

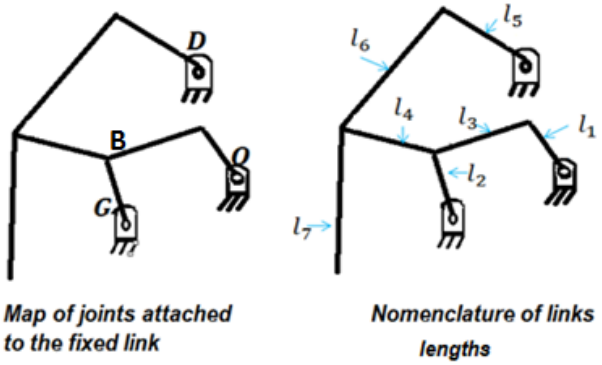

Figure 3

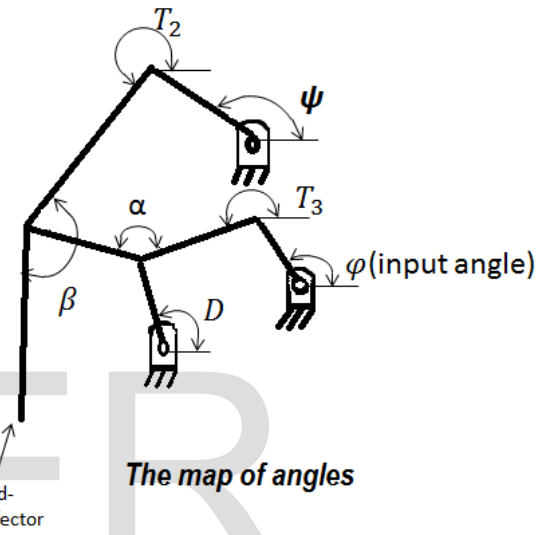

Figure 4

III. Equations to solve the problem

By using polar complex equations ,position of joint B = $\boldsymbol{l_1.e^{i.\varphi} + l_3.e^{iT_1} = (x_g + iy_g) + l_2.e^{iD}}$ → (equation i)

Position of C = $\boldsymbol{B + l_4^{iT_3} = (x_d + iy_d) + l_5.e^{i\psi} + l_6.e^{iT_2}}$ (Where **B** is the polar vector position of point B according to figure 2.)

On substituting $\boldsymbol{T_3 = a + T_2 - \pi}$, the equation above becomes ,

$\boldsymbol{=> B + l_4^{i(a+T_1-\pi)} = (x_d + iy_d) + l_5.e^{i\psi} + l_6.e^{iT_2}}$ →(equation ii)

Solving equation (i) by taking $l_2\ e^{i\,D}$ on one side and all the other terms on the other side , then multiplying the corresponding terms of each side with the equation formed by taking conjugate of $l_2\ e^{i\,D}$ on either side of the equation , we eliminate the term e^{iD} as performed below :

$\boldsymbol{l_2.e^{iD} = l_1.e^{i.\varphi} + l_3.e^{iT_1} - (x_g + iy_g)}$ → (Re-arranged equation i)

$\boldsymbol{\overline{l_2.e^{iD}} = \overline{l_1.e^{i.\varphi}} + \overline{\overline{l_3.e^{iT_1}}} - (\overline{x_g + iy_g})}$ →(Taking conjugate over the entire equation i)

Multiplying the above two equation and equating the real parts , we get :

$$\begin{aligned}=> &\left[(2.l_1.l_3\cos\varphi) - (2.l_3.x_g)\right]\cos T_1 \\ &+\left[(2.l_1.l_3\sin\varphi)\right. \\ &\left.-(2.l_3.y_g)\right]\sin T_1 - [\,l_1^2 + l_3^2 + x_g^2 \\ &+ y_g^2 - l_2^2 - 2.l_1.x_g.\cos\varphi \\ &- 2.l_1.y_g.\sin\varphi] = 0\end{aligned}$$

On solving for $\boldsymbol{T_1}$:

$\boldsymbol{A_1 = (2.l_1.l_3\cos\varphi) - (2.l_3.x_g)}$

$\boldsymbol{B_1 = (2.l_1.l_3\sin\varphi) - (2.l_3.y_g)}$

$$\boldsymbol{C_1 = l_1^2 + l_3^2 + x_g^2 + y_g^2 - l_2^2 - 2.l_1.x_g.\cos\varphi - 2.l_1.y_g.\sin\varphi}$$

$$\boldsymbol{T_1 = 2.\tan^{-1}\left[\frac{\left(B_1 + \sqrt[2]{A_1^2 + B_1^2 - C_1^2}\right)}{(A_1 - C_1)}\right]}$$

Solving equation (i) by taking $l_3\ e^{i\,T_1}$ on one side and all the other terms on the other side , then multiplying the corresponding terms of each side with the equation formed by taking conjugate of $l_3\ e^{i\,T_1}$ on either side of the equation , we eliminate the term e^{iT_1} . On equating the real parts and solving for **D** , we get :

$\boldsymbol{A_2 = 2.l_2.x_g - 2.l_1.l_2.\cos\varphi}$

$\boldsymbol{B_2 = 2.l_2.x_g - 2.l_1.l_2.\sin\varphi}$

$$\boldsymbol{C_2 = l_1^2 + l_2^2 + x_g^2 + y_g^2 - l_3^2 - 2.l_1.x_g.\cos\varphi - 2.l_1.y_g.\sin\varphi}$$

$$\boldsymbol{D = 2.\tan^{-1}\left[\frac{\left(B_2 + \sqrt[2]{A_2^2 + B_2^2 - C_2^2}\right)}{(A_2 - C_2)}\right]}$$

Let P and Q be two variables that assumes the value :

$\boldsymbol{P = l_2.\cos D + l_4.\cos(a + T_1 - \pi) - x_d + x_g}$

$\boldsymbol{Q = l_2.\sin D + l_4.\sin(a + T_1 - \pi) - y_d + y_g}$

On substituting the value of P and Q in equation (ii) , equation (ii) takes the following form :

$l_6.e^{iT_2} = P + iQ - l_5.e^{i\psi}$ → (Substituted in equation ii)

Solving equation (ii) by taking $l_6\ e^{i\,T_2}$ on one side and all the other terms on the other side, then multiplying the corresponding terms of each side with the equation formed by taking conjugate of $l_6\ e^{i\,T_2}$ on either side of the equation , we eliminate the term e^{iT_2} . On equating the real parts and solving for **,** we get :

$\boldsymbol{A_3 = 2.P.l_5}$

$\boldsymbol{B_3 = 2.Q.l_5}$

$\boldsymbol{C_3 = l_6^2 - P^2 - Q^2 - l_5^2}$

$$\boldsymbol{\psi = 2.\tan^{-1}\left[\frac{\left(B_3 - \sqrt[2]{A_3^2 + B_3^2 - C_3^2}\right)}{(A_3 - C_3)}\right]}$$

Solving equation (ii) by taking $l_5\ e^{i\,\psi}$ on one side and all the other terms on the other side, then multiplying the corresponding terms of each side with the equation formed by taking conjugate of $l_5\ e^{i\,\psi}$ on either side of the equation, we eliminate the term $e^{i\psi}$. On equating the real parts and solving for T_2 , we get:

$A_4 = 2.P.l_6$

$B_4 = 2.Q.l_6$

$C_4 = l_5^2 - P^2 - Q^2 - l_6^2$

$$T_2 = 2.\tan^{-1}\left[\frac{\left(B_4 + \sqrt[2]{A_4^2 + B_4^2 - C_4^2}\right)}{(A_4 - C_4)}\right]$$

From figure 1 , the x and y co-ordinate of the end effector respectively are :

$$X = l_5.\cos\psi + l_6.\cos T_2 + l_7.\cos(\pi - b + T_2) + x_d$$

$$Y = l_5.\sin\psi + l_6.\sin T_2 + l_7.\sin(\pi - b + T_2) + y_d$$

X and Y defines the co-ordinate of the end-effector. The trajectory of the Klann mechanism has been simulated on **Matcad** , using the set of equations mentioned above . Different cases of gaits pertaining to debris removal and excavation has been explored.

CASE I : On taking , $l_1 = 24, l_2 = 33 , l_3 = 63, x_g = -58 , y_g = -14 , l_4 = 50 , a = 160° , l_5 = 50 , l_6 = 45, b = 160° , l_7 = 110 , x_d = -50 , y_d = 30$, we are able to generate the *default trajectory* for the *end-effectors* of the Klann mechanism(Fig 5).

CASE II : On taking : $l_1 = 24, l_2 = 30 , l_3 = 64, x_g = -58 , y_g = -14 , l_4 = 57 , a = 160° , l_5 = 77 , l_6 = 80, b = 160° , l_7 = 110 , x_d = -50 , y_d = 30$, we are able to generate the *digging motion trajectory* for the *end-effectors* of the Klann mechanism(Fig 6).

CASE III : On taking : $l_1 = 24, l_2 = 44 , l_3 = 75, x_g = -58 , y_g = -14 , l_4 = 70 , a = 160° , l_5 = 80 , l_6 = 40, b = 160° , l_7 = 140 , x_d = -50 , y_d = 30$, we are able to generate the *striking motion trajectory* for the *end-effectors* of the Klann mechanism(Fig 7).

CASE IV : On taking : $l_1 = 24, l_2 = 44 , l_3 = 75, x_g = -58 , y_g = -14 , l_4 = 70 , a = 160° , l_5 = 80 , l_6 = 50, b = 160° , l_7 = 140 , x_d = -50 , y_d = 30$, we are able to generate the *scrounging motion trajectory* for the *end-effectors* of the Klann mechanism(Fig 8).

CASE V : On taking : $l_1 = 24, l_2 = 44 , l_3 = 75, x_g = -58 , y_g = -14 , l_4 = 70 , a = 160° , l_5 = 85 , l_6 = 80, b = 160° , l_7 = 110 , x_d = -50 , y_d = 30$, we are able to generate the *hammering motion trajectory* for the *end-effectors* of the Klann mechanism(Fig 9).

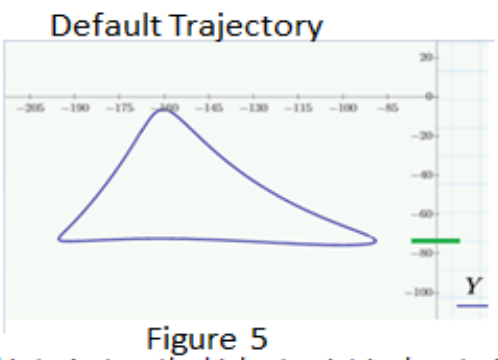

Figure 5

In this trajectory the highest point is close to 60 % of length of the step. More height has been considered to avoid un-necessary debris at excavation sites. The horizontal region marks the level of ground that is used for reference in other gaits.

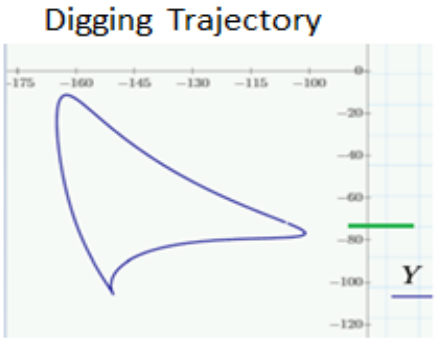

Figure 6

This trajectory extend way beyond the ground level. This gait is useful in excavation and removal of debris irrespective of the presence or absence of a pit

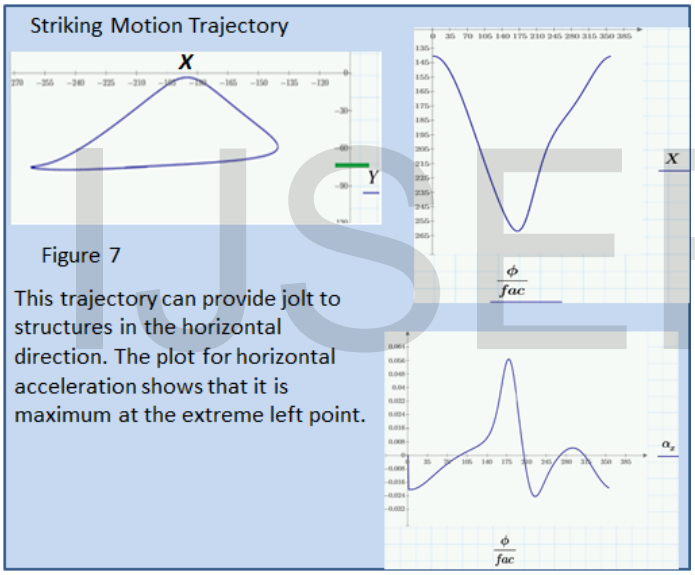

Figure 7

This trajectory can provide jolt to structures in the horizontal direction. The plot for horizontal acceleration shows that it is maximum at the extreme left point.

Scrounging motion trajectory

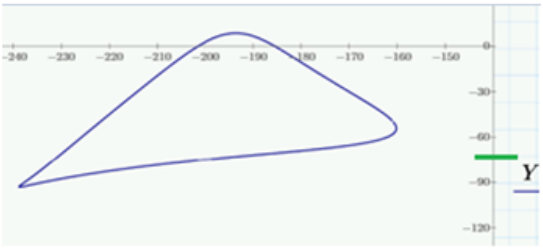

Figure 8

This trajectory essentially is to seek or scrape over heaps of material to draw it close.

Hammering motion trajectory

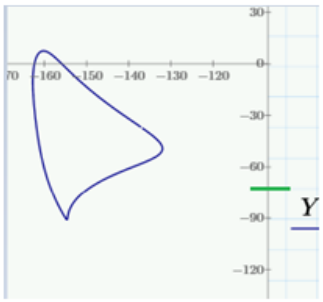

Figure 9

This trajectory is the extreme case of digging. In this trajectory the horizontal displacement has reduced in comparison to the trajectory for digging. The robot does not move much. It remains at the same position and repeatedly strikes there to crumble the hard ground.

IV. Programming the problem on Mathcad

Since programming on Mathcad allows us to take angle in radian the input angle ϕ in degrees is defined in terms of a variable *fac* . Since the input angle ϕ changes its value , it has been considered as a vector with values varying over a range from 1 to 360 :

$fac = \frac{\pi}{180},\ i = 1..360\ ,\ \varphi_i$ = (i-1).fac

The x co-ordinate and the y co-ordinate (***X , Y***) are function of input variable φ_i , which changes as i varies between 1 to 360. The time elapsed by the time the input angle φ_i changes from 0° to (i-1)° is defined by , t_i , where $t_i = \frac{i-1}{\omega}$ and ω is the angular velocity in radians/minute.

$$V_{x_j} = \frac{(X_{j+1} - X_{j-1})}{(t_{j+1} - t_{j-1})},$$

$$V_{y_j} = \frac{(Y_{j+1} - Y_{j-1})}{(t_{j+1} - t_{j-1})}$$

V_x and V_y are the velocities in the x and y direction respectively

$$\alpha_{x_j} = \frac{\left(V_{x_{j+1}} - V_{x_{j-1}}\right)}{(t_{j+1} - t_{j-1})}$$

$$\alpha_{y_j} = \frac{\left(V_{y_{j+1}} - V_{y_{j-1}}\right)}{(t_{j+1} - t_{j-1})}$$

α_x and α_y are the linear acceleration in the x and y direction respectively.

V. Inferences drawn

For Case II , the curve for α_x and α_y are :

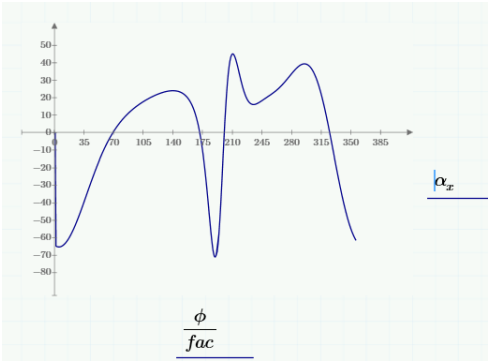

Figure 10

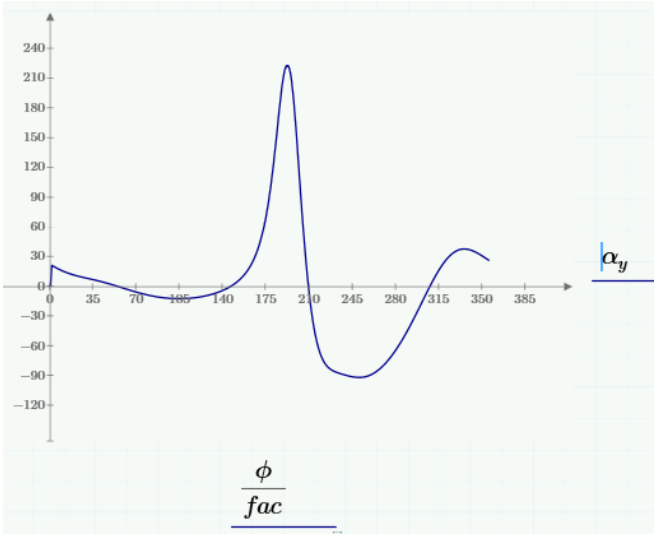

Figure 11

The linear acceleration in the y-direction (α_y) is maximum at 194° .On plotting the curve between the ω (input angular velocity) and the $\alpha_{y_{max}}$, it has been observed that the value of $\alpha_{y_{max}}$ increases quadratically with increase in ω.

X Axis Title (ω)	Y Axis Title ($\alpha_{y_{max}}$)
1	0.089
5	2.227
10	8.91
100	890.984
500	22270
1000	89100
10000	8910000
5000	2227000

Table 1

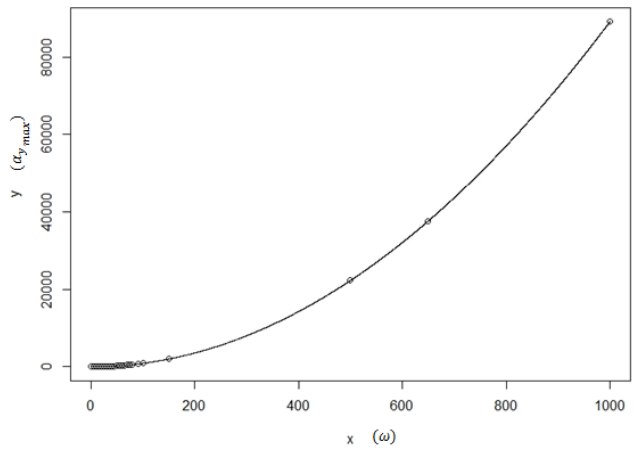

Figure 12

On using **quadratic regression method** of fitting the data-points , the equation of the curve was found to be y = **0.0891**x^2 with maximum percentage error of 0.1 % at the first point.

On using **cubic regression** the coefficient of x^3 is extremely small and its contribution is negligible.

y = -2.334079 + 0.04317026 x + 0.08904724x^2 + 847044e-9x^3

The co-efficient of x and x^2 are comparable and several orders greater than the co-efficient of x^3 , hence the acceleration curve can essentially be considered quadratic.

It can be inferred from Figure 9 that vertical impact for digging will increase following a quadratic curve.

For Case IV **,** The curve for α_x and α_y are:

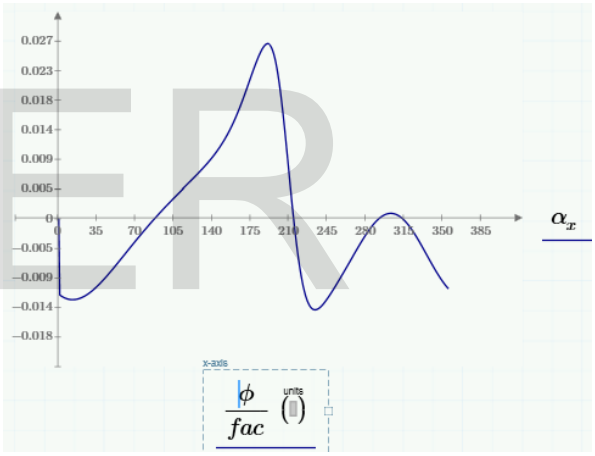

Figure 13

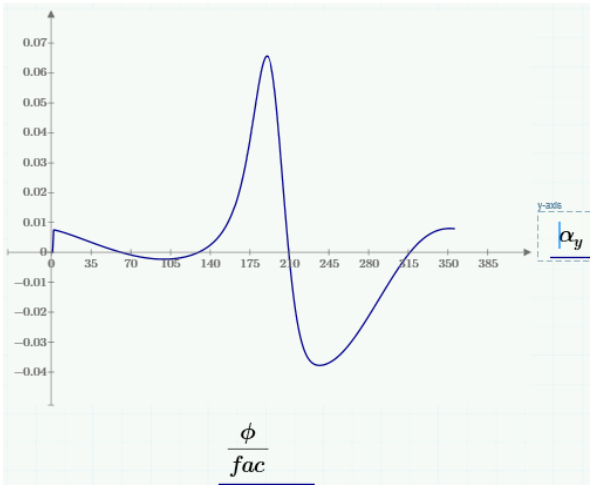

Figure 14

The linear acceleration in the y-direction (α_y) and x-direction (α_x) is maximum at 191° and 192° respectively. Table 2 shows the plot of ω against $\alpha_{y_{max}}$.

X Axis Title (ω)	Y Axis Title ($\alpha_{y_{max}}$)
1	0.066
5	1.643
10	6.571
20	26.285
100	657.126
500	16430
1000	65710
5000	1643000
10000	6571000

Table 2

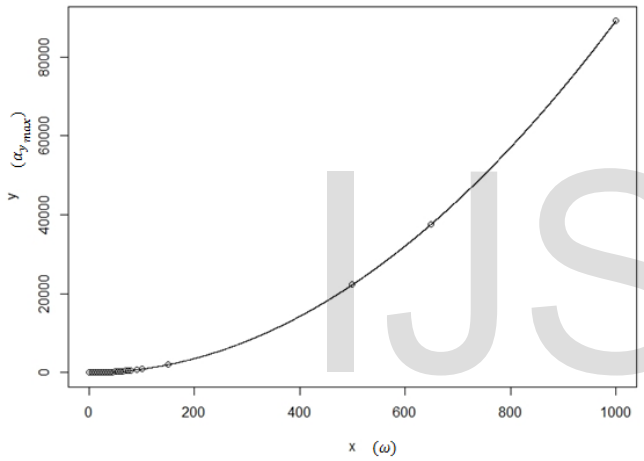

Figure 15

On using **quadratic regression method** of fitting the data-points , the equation of the curve was found to be $\boldsymbol{y = 0.06571x^2}$ with maximum percentage error of 0.4 % at the first point.

The equation for the **cubic regression method** best-fit curve for $\alpha_{y_{max}}$ against ω is :

$\boldsymbol{y = 1.017991 - 0.02134618x + 0.06573632x^2 - 2.419626e\text{-}9x^3}$

The co-efficient of x and x^2 are comparable and several orders greater than the co-efficient of x^3 , hence the acceleration curve can essentially be considered quadratic.

If ω is a linear function in time then linear acceleration is a quadratic function in time and the ω versus α curve is quadratic in nature. This implies , ω versus *V* is a cubic curve and ω versus *X* or *Y* is a bi-quadratic curve. This also means φ versus *X or* φ versus *Y* is a curve of the fifth order. Thus to define the trajectory of the end-effector of the Klann mechanism whose input link has constant acceleration or deceleration , a fifth order equation in time is required .

The $\alpha_{y_{max}}$ is a measure of the vertical impact force that the end-effector imparts on the ground and itself experiences as a reaction. This analysis helps in understanding how the impact force varies with change in the input angular velocity (ω). A choice of material to design the linkages and the end effector can also be made if the range of the rpm of the input motors are known.

VI. CONCLUSION

A original design approach has been presented in this paper towards the development of trajectory generator that takes the length of the links as input and plots the trajectory with change in the input angle φ .These trajectories can be realized with reconfigurable links .Although not all the links of the Klann mechanism can be made reconfigurable we were able to confirm that various gaits pertaining to debris removal is achievable from a single set of robotic leg based on reconfigurable links . All these trajectories are salient curves with regard to the kind of operation the robot will perform. It has also been found that all these trajectories has its substantial lower portion in contact with the ground marked in green along the Y-axis in Figure 5 through till Figure 9. This indicates that the trajectories are compatible with not much change in the height of the platform when the legs change the gaits from one form to the other. While designing the linkages and choosing the motors it must be realized that the impact force changes following a quadratic curve with the rpm of the motor. All trajectories for gaits of debris removal has a point on the acceleration curve where its value is maximum. They are also the point in the trajectory where the end-effector makes the greatest impact with the environment. Many more useful trajectories can be created with intermediate link lengths apart

from the ones identified. The link lengths provided in this work can act as a guideline for generating these trajectories at various scales where each of the dimensions can be proportionally changed.

VII. REFERENCES

1. Kajita , S . ; Espiau , B . Legged robots. In handbooks of Robotics ; Siciliano, B., Khatib, O., Eds.; Springer: Berlin/Hidelberg, Germany ,2008.
2. C. Paul, Morphological computation: a basis for the analysis of morphology and control requirements, Robot. Auton. Syst. 54 (8) (2006) 619–630.
3. Pal, P.K.; Jayarajan, K. Generation of free gait-a graph search approach. IEEE Trans. Robot. Autom. 1991, 7, 299–305
4. Asano, F.; Yamakita, M.; Kamamichi, N.; Luo, Z.W. A novel gait generation for biped walking robots based on mechanical energy constraint. IEEE Trans. Robot. Autom. 2004, 20, 565–573.
5. Shuuji KAJITA, Fumio KANEHIRO, Kenji KANEKO, Kiyoshi FUJIWARA, Kensuke HARADA, Kazuhito YOKOI and Hirohisa HIRUKAWA :Biped Walking Pattern Generation by using Preview Control of Zero-Moment Point
6. Sheba, J.K.; Mohan, R.E.; Martínez-García, E.; Tan-Phuc, L. Synthesizing reconfigurable foot traces using a Klann mechanism. Robotica 2015, 1–17
7. Jaichandar Kulandaidaasan Sheba , Mohan Rajesh Elara , Edgar Martínez-García and Le Tan-Phuc : Trajectory Generation and Stability Analysis for Reconfigurable Klann Mechanism Based Walking Robot
8. Seonhyeok Kang , Jae Mann Park , Seunghyun Kim , Bong-ju Lee , Youngbum Kim , Panyoung Kim , Hyoun Jin Kim : Path tracking for a hydraulic excavator utilizing proportional-derivative and linear quadratic control.
9. 8. F. I. Sheikh and R. Pfeifer, “Adaptive locomotion on varying ground conditions via a reconfigurable leg length hopper”, Adaptive Mobile Robotics, 527-535 (2012).